

# Directional shift current in mirror-symmetric BC<sub>2</sub>N

Julen Ibañez-Azpiroz,<sup>1</sup> Ivo Souza,<sup>1,2</sup> and Fernando de Juan<sup>2,3</sup>

<sup>1</sup>*Centro de Física de Materiales, Universidad del País Vasco (UPV/EHU), 20018 San Sebastián, Spain*

<sup>2</sup>*Ikerbasque Foundation, 48013 Bilbao, Spain*

<sup>3</sup>*Donostia International Physics Center (DIPC), 20018 San Sebastián, Spain*

(Dated: June 19, 2019)

We present a first-principles theoretical study of the shift current in a noncentrosymmetric polytype of graphitic BC<sub>2</sub>N, and find that the photoconductivity exhibits two distinctive features at the band edge. First, it ranks among the largest bulk nonlinear responses reported to date, with the peak value occurring in an energy range suitable for optical manipulation. Secondly, it is strongly anisotropic, due to the vanishing of particular tensor components not foretold by phenomenological symmetry arguments; this is a consequence of dipole selection rules imposed by mirror symmetry, which imply that the relative parities between valence and conduction bands are key for determining the directionality of the band-edge response. Our work identifies graphitic BC<sub>2</sub>N as a promising candidate for next-generation photovoltaics, and opens up a broad framework for future studies.

*Introduction* – The conversion of light into electrical current via the photovoltaic effect is one of the most copious supplies of renewable energy on Earth. Traditional solar cells make use of *p-n* junctions to generate a built-in electric field that drives the photoexcited electrons. It has long been known that single-phase noncentrosymmetric crystals exhibit a different type of photovoltaic effect, called the *bulk photovoltaic effect* (BPVE) [1–3]. This is a nonlinear optical response that consists in the generation of a photovoltage (open circuit) or photocurrent (closed circuit) when light is absorbed via intrinsic or extrinsic processes. Since the BPVE occurs in homogeneous systems, it needs no sophisticated interface-engineering techniques for its usage as sunlight harvester. As further appealing features of the BPVE, the photovoltage is not limited by the band gap of the material, nor is device performance constrained by the Shockley-Queisser limit that applies to conventional solar cells [4]. In the past few years, the study of the BPVE for solar-cell applications has been reinvigorated by the search for novel materials with large photoresponsivities [5–7]. There is also renewed interest on more fundamental aspects of the BPVE, particularly its sensitivity to the geometric and topological properties of the electronic wave functions [8–10].

Recently, considerable attention has been paid to the directionality of the BPVE, namely to the relative orientation and size of the generated photocurrent as a function of the polarization of light. As an example, the sign of the shift-current contribution to the BPVE has been suggested as a possible probe for detecting topological phase transitions [11, 12]. In addition, recent experimental work on the Weyl semimetal TaAs found large and anisotropic contributions to the shift-current BPVE driven by the low-energy Weyl-node physics [13].

In this work, we report a distinctive shift-current response at the band edge of a noncentrosymmetric polytype of graphitic BC<sub>2</sub>N, a layered semiconductor made of alternating zigzag chains of carbon and boron nitride [14–

20]. Our *ab initio* calculations reveal two unusual features of the shift-current spectrum near the fundamental band gap. First, its peak magnitude ranks amongst the largest bulk nonlinear responses reported to date. In addition, the calculated response reveals a strong anisotropy due to the vanishing of certain tensor components not foretold by phenomenological symmetry arguments. This allows, for example, to engineer particular conditions where the current flows perpendicularly to the applied field. We trace the origin of this anisotropy to the mirror symmetry of the crystal structure, which imposes selection rules on dipole transitions between the top of the valence band and the bottom of the conduction band. We capture the essential physics of this phenomenon by generalizing a two-band tight-binding model introduced in Ref. 21, thus providing a suitable framework for a broad class of materials.

*Shift-current BPVE* – The BPVE is a nonlinear optical response of the form [1]

$$J_a = \sum_{b,c} \sigma^{abc}(\omega) E_b(\omega) E_c(-\omega), \quad (1)$$

where  $a$ ,  $b$ , and  $c$  are Cartesian indices. Since both the electric field  $\mathbf{E}$  and the current  $\mathbf{J}$  are odd under inversion, the two sides of Eq. (1) pick up opposite signs under this symmetry; hence, the BPVE can only occur in systems where inversion symmetry is broken. The right-hand side of Eq. (1) can be split into symmetric and antisymmetric parts under  $b \leftrightarrow c$ , known respectively as the *linear* and *circular* BPVE [1]; the former occurs in piezoelectric crystals, and the latter in gyrotropic crystals. The shift current is the intrinsic (interband) contribution to the linear BPVE.

In the independent-particle picture, the shift-current contribution to the photoconductivity in Eq. (1) takes the form [22]

$$\sigma^{abc}(\omega) = C \int \frac{d^3k}{(2\pi)^3} \sum_{n,m} f_{nm} I_{mn}^{abc} \delta(\omega_{nm} - \omega), \quad (2)$$

where  $C = -\pi g_s |e|^3 / 2\hbar^2$  is a combination of fundamental constants ( $g_s = 2$  accounts for the spin degeneracy),  $f_{nm} = f_n - f_m$  and  $\hbar\omega_{nm} = E_n - E_m$  are differences in band occupations and band energies, and the matrix element reads

$$I_{mn}^{abc} = \text{Im} (r_{mn}^b r_{nm}^{c;a}) + b \leftrightarrow c. \quad (3)$$

Here  $r_{mn}^b$  is the interband dipole (the off-diagonal part of the Berry connection matrix  $A_{mn}^b = i\langle u_{m\mathbf{k}} | \partial_{k_b} u_{n\mathbf{k}} \rangle$ ) which only depends on the initial and final states  $m$  and  $n$ , and  $r_{nm}^{c;a}$  is a generalized derivative defined as  $r_{nm}^{c;a} = \partial_{k_a} r_{nm}^c - i(A_{nn}^a - A_{mm}^a) r_{nm}^c$ , which depends implicitly on intermediate virtual states [22]. Like the intrinsic anomalous Hall effect in ferromagnets [23], the shift current arises from purely interband velocity matrix elements and probes the intrinsic Berry-phase geometry of the Bloch bands [21, 22, 24, 25].

*Mirror symmetry and the role of band-edge parities* – We next analyze the constraints imposed on the form of the shift photoconductivity tensor by the presence of mirror symmetry; without loss of generality, we take that symmetry to be  $M_x : x \rightarrow -x$ . If  $M_x$  leaves the crystal structure invariant, then according to Eq. (1) the tensor  $\sigma^{abc}$  can be nonzero only when  $x$  appears an even number of times (zero or two) in  $abc$ . This is a phenomenological constraint, which holds at any frequency and irrespective of the mechanism behind the BPVE; it also holds if the space-group operation is not a pure reflection but a glide.

Now assume that the space-group operation is a pure reflection  $M_x$ , and that the minimum direct gap  $E_g = E_c - E_v$  is located on a  $M_x$ -invariant plane in the BZ. Under these conditions, the shift photoconductivity at frequencies close to  $E_g$  is further restricted by dipole selection rules, in much the same way as the absorptive part of the linear conductivity [26, 27]. The reason is that the states  $|v\rangle$  and  $|c\rangle$  at the top of the valence band and at the bottom of the conduction band are now eigenstates of  $M_x$ , with eigenvalues  $\pm i$  in the spinful case and  $\pm 1$  in the spinless case; introducing a “relative mirror parity”  $\mathcal{P}_{vc}^x$  that equals  $+1$  ( $-1$ ) when  $|v\rangle$  and  $|c\rangle$  have equal (opposite) eigenvalues, the dipole matrix elements are found to satisfy [26, 27]

$$r_{vc}^x = 0, \text{ when } \mathcal{P}_{vc}^x = +1, \quad (4a)$$

$$r_{vc}^y = r_{vc}^z = 0, \text{ when } \mathcal{P}_{vc}^x = -1. \quad (4b)$$

By virtue of Eqs. (2) and (3), these selection rules set some components of  $\sigma^{abc}(\omega)$  to zero for  $\hbar\omega \approx E_g$ .

Let us first consider the shift current induced by light with linear polarization along  $b = c$ . In this case, the phenomenological constraint mentioned above becomes  $\sigma^{xbb} = 0$ , and so the current must flow parallel to the mirror plane (we will refer to this as “in-plane flow”). Concerning the band-edge response, one can distinguish two scenarios on the basis of Eq. (4). When  $\mathcal{P}_{vc}^x = +1$  the matrix element  $I_{mn}^{abb}$  vanishes for  $b = x$  so that  $\sigma^{axx} =$

TABLE I. Selection rules for the band-edge shift photoconductivity  $\sigma^{abc}(\hbar\omega \approx E_g)$  in the crystal class  $mm2$ , when the two reflection operations are not glides. Each column lists one of the symmetry-allowed components of the photoconductivity tensor, followed by the relative  $M_x$  and  $M_z$  parities of the valence and conduction band-edge states that allow that component to be non-negligible for  $\hbar\omega \approx E_g$ . The relative parities for BC<sub>2</sub>N-A2,  $\mathcal{P}_{vc}^x = -1$  and  $\mathcal{P}_{vc}^z = +1$ , are marked in bold; they imply that only  $\sigma^{yxx}$  and  $\sigma^{xxy}$  (also marked in bold) are non-negligible at the band edge of this material.

	Components of $\sigma^{abc}(\hbar\omega \approx E_g)$				
	<b><math>yxx</math></b>	<b><math>xxy=xyx</math></b>	$yyy$	$yzz$	$zzy=zyz$
$\mathcal{P}_{vc}^x$	<b>-1</b>	<b>+1/-1</b>	+1	+1	+1
$\mathcal{P}_{vc}^z$	<b>+1</b>	<b>+1</b>	<b>+1</b>	-1	<b>+1/-1</b>

0, and when  $\mathcal{P}_{vc}^x = -1$  it vanishes for  $b \neq x$  so that  $\sigma^{ayy} = \sigma^{azz} = 0$ . Thus, when  $\mathcal{P}_{vc}^x = +1$  ( $\mathcal{P}_{vc}^x = -1$ ) the shift current flows in response to the in-plane (out-of-plane) component of the optical electric field; in both cases, it flows strictly in-plane. We emphasize that this sharp separation only occurs at the band edge.

To complete the present discussion, let us consider the possible contributions to the shift current from  $\sigma^{abc}$  with  $b \neq c$ . Such contributions average to zero for unpolarized light (*e.g.*, sunlight), which is why those tensor components are often ignored when discussing potential solar-cell applications of the BPVE [6, 21, 28]. When they are present, the current is no longer constrained to flow in-plane. At the band edge,  $\mathcal{P}_{vc}^x = +1$  does not impose any restriction at all while  $\mathcal{P}_{vc}^x = -1$  forces  $\sigma^{abc}$  to vanish if both  $b \neq x$  and  $c \neq x$ .

*Physical realization* – We now show that graphitic BC<sub>2</sub>N provides a striking illustration of the preceding discussion. We begin by noting that while a single layer breaks inversion symmetry [see Fig. 1(a)], whether inversion is still broken in the bulk structure depends on the stacking pattern, which remains to be determined experimentally. There are two types of stackings, denoted A or B depending on whether consecutive layers have the same or opposite orientation [29]. B-type structures have a center of inversion between the layers, while those of type A break inversion symmetry. As a result, the photoconductivity vanishes in B-type structures but remains finite in those of type A.

We consider the most stable A-type bulk structure identified in Ref. 29, namely the A2 structure illustrated in Fig. 1(a). The space group is  $Pmm2$  (No. 25), and the point group is  $mm2$ . There are two mirrors  $M_x$  and  $M_z$ , and a rotation  $C_2^y$  about the polar axis. Point-group symmetry allows five out of nine components of the linear BPVE tensor  $\sigma^{abc} = \sigma^{acb}$  to be nonzero: three involving in-plane directions only ( $yxx$ ,  $xxy = xyx$ , and  $yyy$ ), and two that also involve  $z$  ( $yzz$  and  $zzy = zyz$ ). Since  $M_x$  and  $M_z$  are pure reflections, at the band edge further re-

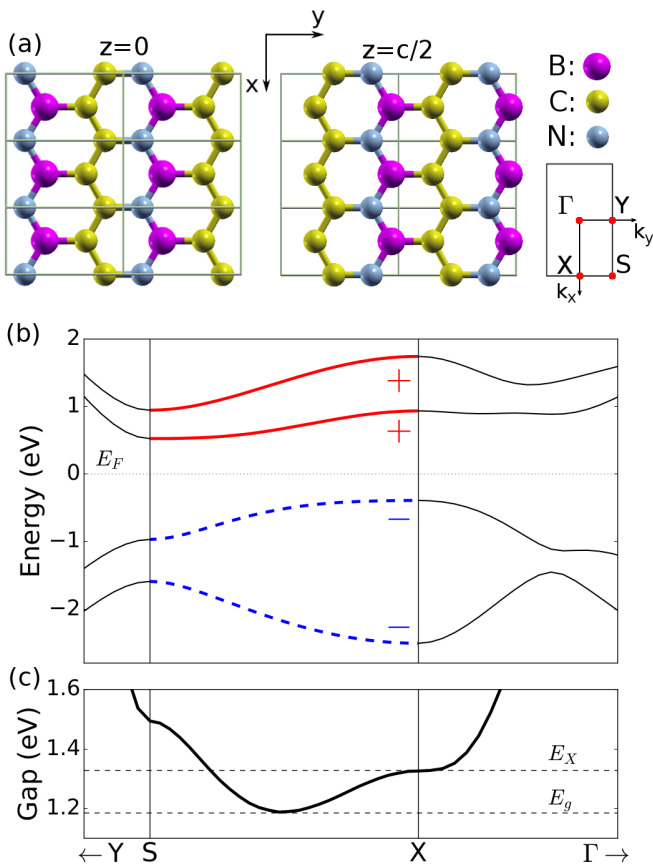


FIG. 1. (a) Two adjacent layers of the  $\text{BC}_2\text{N-A2}$  structure, with two formula units per cell of height  $c$ . The B, C and N atoms are represented by magenta, yellow and blue balls respectively, and the solid gray lines delimit the cells (the horizontal lines coincide with one family of  $M_x$  symmetry planes). The 2D BZ is also illustrated. (b) Band structure on the  $k_z = 0$  plane, with energies measured from the Fermi level. Along S-X, thick solid (red) and dashed (blue) lines denote bands with  $M_x$  eigenvalues  $+1$  and  $-1$ , respectively, while along other symmetry lines all bands are drawn as thin solid lines. (c) Direct band gap, with values  $E_g$  and  $E_X$  at the band edge and at X, respectively.

restrictions emerge from dipole selection rules as detailed in Table I.

The scalar-relativistic band structure of  $\text{BC}_2\text{N-A2}$  near the band edge is displayed in Fig. 1(b). We only show the dispersion on the  $k_z = 0$  plane because the weak interlayer coupling produces a quasi-2D band structure with virtually no  $k_z$  dispersion [29]. Inspection of the figure reveals that the dispersion from S to X is also relatively weak. The minimum direct band gap of  $E_g \approx 1.18$  eV is located approximately midway between those two time-reversal invariant momenta (TRIM), as shown in Fig. 1(c). On the S-X line, whose points remain invariant under  $M_x$ , the energy eigenstates are also eigenstates of  $M_x$ , with eigenvalues  $\pm 1$  as depicted by the solid and dashed lines in Fig. 1(b). We have explicitly verified that

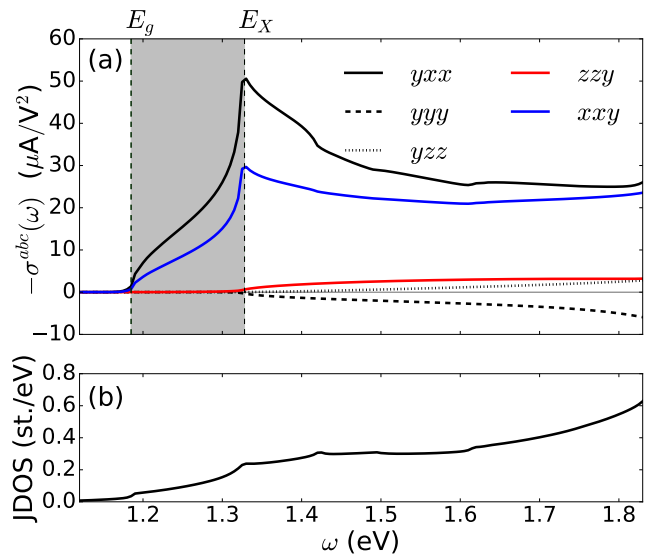


FIG. 2. (a) Shift photoconductivity of bulk  $\text{BC}_2\text{N-A2}$  calculated *ab initio*. The gray area indicates the band-edge energy range from  $E_g$  to  $E_X$  [see Fig. 1(c)]. (b) Calculated JDOS.

the upper-valence and lower-conduction bands have opposite  $M_x$  eigenvalues, *i.e.*,  $\mathcal{P}_{vc}^x = -1$ . Moreover, since all bands in Fig. 1(b) are derived from  $p_z$ -type Wannier functions (see below), they all have the same  $M_z$  eigenvalue  $-1$  on the  $k_z = 0$  plane, so that  $\mathcal{P}_{vc}^z = +1$ . With these two parity values in hand, we can consult Table I to find out which components of the shift photoconductivity tensor are expected to be present at the band edge.

We have computed the shift photoconductivity of  $\text{BC}_2\text{N-A2}$  by means of density-functional theory (DFT). The calculations were performed using the **Quantum ESPRESSO** code package [30], taking the structural parameters from Ref. 29. The core-valence interaction was treated using scalar-relativistic projector augmented-wave pseudopotentials constructed using the Perdew-Burke-Ernzerhof exchange-correlation functional [31]. The self-consistent calculations were carried out on a  $10 \times 10 \times 10$   $k$ -point mesh with the plane-wave cutoff set at 60 Ry. In a post-processing step, maximally-localized Wannier functions [32, 33] were generated with the **Wannier90** package [34], starting from atom-centered  $p_z$  trial orbitals to model the bands around the Fermi level. Finally, the photoconductivity was calculated using a recently-developed Wannier-interpolation scheme [35].

The calculated photoconductivity is shown in Fig. 2(a). As predicted in Table I, three of the five symmetry-allowed components,  $\sigma^{yyy}$ ,  $\sigma^{zzy}$  and  $\sigma^{yzz}$ , have negligible values in the band-edge region indicated by the gray area. The other two,  $\sigma^{yxx}$  and  $\sigma^{xxy}$ , grow rapidly from the onset at  $E_g$  until reaching peak values of  $\sigma^{yxx} \sim 50 \mu\text{AV}^{-2}$  and  $\sigma^{xxy} \sim 30 \mu\text{AV}^{-2}$  at  $E_X \approx 1.33$  eV; above  $E_X$  they drop gradually and then stabilize at roughly half their peak values, before peaking again near 2 eV (not shown).

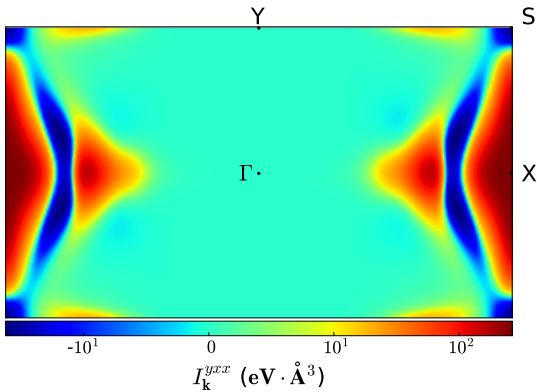


FIG. 3. Heatmap plot across the 2D BZ at  $k_z = 0$  of the matrix element  $I_{\mathbf{k}}^{yxx} = \sum_{m,n} I_{mn\mathbf{k}}^{yxx}$  describing the shift-current response near the band edge of bulk g-BC<sub>2</sub>N-A2 (transitions far from the band edge are excluded by restricting the summations to the upper-valence and lower-conduction bands).

The three previously-negligible components become sizeable above  $E_X$  due to contributions from valence and conduction bands outside the mirror-invariant S–X line [see Figs. 1(b,c)], but they remain small compared to the other two.

For light with linear polarization along a crystallographic axis [ $b = c$  in Eq. (1)], the spectrum in Fig. 2(a) can be rationalized as follows on the basis of the symmetry arguments discussed previously. At all frequencies  $\hbar\omega > E_g$  the shift current flows along the line of intersection between the two mirror planes (along  $y$ ), and at band-edge frequencies it only flows in response to the field component along  $x$  (normal to the  $M_x$  mirror with  $P_{vc}^x = -1$ , and parallel to the  $M_z$  mirror with  $P_{vc}^z = +1$ ).

Having understood the directionality of the BPVE at the band edge of BC<sub>2</sub>N-A2, we now examine the origin of the strong peak in  $\sigma^{yxx}$  at  $E_X$ . The peak value is comparable to the largest reported photoconductivity for a gapped material,  $\sigma^{zzz} \sim 50 \mu\text{AV}^{-2}$  in ferroelectric PbTiO<sub>3</sub> at 6 eV [36]. In addition, it occurs at a frequency of  $\hbar\omega \approx 1.3$  eV that is suitable for optical manipulation, and where bulk semiconductors typically have much smaller responses [6, 37, 38]. (In experiment the peak is likely to occur at a higher energy in the visible range, due to the typical band-gap underestimation in DFT; for the B12 polytype of BC<sub>2</sub>N, that underestimation is around 0.6 eV [29]). The Glass coefficient [6, 39], which quantifies photocurrent generation in bulk materials taking absorption into account, peaks at the same frequency as the shift current, with a value  $G^{yxx} \sim 3 \cdot 10^{-8}$  cm/V that again ranks among the largest reported to date [13].

To analyze this large response, we write the photoconductivity close to the band edge as the product between the shift-current matrix element and the JDOS [21],

$$\sigma^{abc}(\omega) = C I_{vc}^{abc}(\omega)N(\omega), \quad (5)$$

where the coefficient  $C$  is the same as in Eq. (2). The JDOS, plotted in Fig. 2(b), exhibits a peak at  $E_X$ . That peak is a 2D-like Van Hove singularity due to a saddle point in the direct band gap [see Fig. 1(c)], and it boosts the amount of electronic transitions that contribute to the shift current around that energy. Moreover, those transitions carry a sharply-enhanced matrix element for  $\sigma^{yxx}$ . This can be seen in Fig. 3, which displays a heatmap plot of the matrix element  $I_{mn\mathbf{k}}^{yxx}$  of Eq. (2) summed over the upper-valence and lower-conduction bands: around X, it is more than two orders of magnitude larger than almost anywhere else in the 2D BZ.

*Two-band model in 2D* – Motivated by the quasi-2D nature of graphitic BC<sub>2</sub>N-A2, we now construct a minimal 2D model that captures the effect of mirror parities on the photoconductivity near the band edge. The model lies flat on the  $(x, y)$  plane, and has both  $M_x$  and  $M_z$  symmetry. For simplicity we assume that the band edge is located at a TRIM on a  $M_x$ -invariant line in the 2D BZ, not at a generic point along such a line as in the case of BC<sub>2</sub>N-A2. With these constraints, the most general two-band  $\mathbf{k} \cdot \mathbf{p}$  Hamiltonian that can be obtained by expanding up to second order in  $\mathbf{k} = (k_x, k_y)$  around the TRIM is

$$H(k_x, k_y) = (\alpha_x k_x^2 + \alpha_y k_y^2 + \alpha_{xy} k_x k_y) \sigma_x + (v_x k_x + v_y k_y) \sigma_y + (\Delta + \beta_x k_x^2 + \beta_y k_y^2 + \beta_{xy} k_x k_y) \sigma_z. \quad (6)$$

Essentially the same model was considered in Ref. 21, with the following differences. (i) In Ref. 21 the coordinate system was chosen to eliminate terms linear in  $k_x$ ; instead, we have oriented the axes such that the vertical mirror is  $M_x$ , which requires keeping terms linear in both  $k_x$  and  $k_y$ . (ii) We took as basis states the energy eigenstates at the valence and conduction band edges; as a result, our Hamiltonian is diagonal at  $\mathbf{k} = 0$ .

Since our basis states are also eigenstates of  $M_x$  with eigenvalues  $\pm 1$ , the operator  $M_x$  is represented by the identity matrix when  $\mathcal{P}_{vc}^x = +1$  and by  $\sigma_z$  when  $\mathcal{P}_{vc}^x = -1$ . In a model with translational symmetry,  $M_x$  invariance implies  $M_x H(\mathbf{k}) M_x^{-1} = H(M_x \mathbf{k})$ . When applied to Eq. (6) using the two forms for  $M_x$ , this condition yields

$$v_x = \alpha_{xy} = \beta_{xy} = 0, \quad \text{when } \mathcal{P}_{vc}^x = +1, \quad (7a)$$

$$\alpha_x = \alpha_y = v_y = \beta_{xy} = 0, \quad \text{when } \mathcal{P}_{vc}^x = -1. \quad (7b)$$

The relative band-edge parity  $\mathcal{P}_{vc}^x$  therefore defines two classes of models with very different properties. The model with  $\mathcal{P}_{vc}^x = +1$  was used in Ref. 21 to describe the band-edge photoconductivity of monolayer GeS, while the model with  $\mathcal{P}_{vc}^x = -1$  applies to BC<sub>2</sub>N-A2.

(Regarding  $M_z$  symmetry, the model in Eq. (6) has  $\mathcal{P}_{vc}^z = +1$  because all atomic orbitals have the same parity and lie on the same plane. In this case,  $M_z$  invariance

does not impose any further constraints on the model parameters.)

Starting from the two-band Hamiltonian in Eq. (6), the matrix element in Eq. (5) can be evaluated as described in Refs. 21 and 40. Because the model is purely 2D, the photoconductivity vanishes when any of the three indices equals  $z$ ; on the  $(x, y)$  plane, the nonzero components are

$$I_{vc}^{yyyy}(\omega) = \frac{8v_y\alpha_y\Delta}{\omega^3}, \quad (8a)$$

$$I_{vc}^{xxy}(\omega) = \frac{(4v_y\alpha_x + 2v_x\alpha_{xy})\Delta}{\omega^3} = I_{vc}^{xyx}(\omega), \quad (8b)$$

$$I_{vc}^{yxx}(\omega) = \frac{4v_x\alpha_{xy}\Delta}{\omega^3}. \quad (8c)$$

Using Eq. (7) we find that when  $P_{vc}^x = +1$  the  $yxx$  component vanishes, while for  $P_{vc}^x = -1$  it is the  $yyy$  component that vanishes. These results are in agreement with the first three columns of Table I for the case  $\mathcal{P}_{vc}^z = +1$ .

Besides illustrating the mirror selection rules, our model reveals a simple quantitative relation,

$$\sigma^{yxx} = 2\sigma^{xxy}, \quad \text{when } \mathcal{P}_{vc}^x = -1 \text{ and } \mathcal{P}_{vc}^z = +1, \quad (9)$$

between the two surviving components of the band-edge photoconductivity. The above relation is satisfied rather well by our *ab initio* spectrum throughout the entire band-edge region in Fig. 2(a). This can be understood from the fact that Eq. (9) is quite robust: it follows directly from Eq. (3) once we set  $\mathcal{P}_{vc}^x = -1$  and  $\mathcal{P}_{vc}^z = +1$  in Eq. (4), and use the identity  $r_{cv}^{y;x} = r_{cv}^{x;y}$  that holds for any two-band tight-binding model once off-diagonal position matrix elements are discarded [35].

*Discussion* – To conclude, we discuss the prospects for realizing the physics described herein. The experimental evidence for the stacking sequence in graphitic BC<sub>2</sub>N remains inconclusive [15, 16]. According to DFT calculations, the two most stable polytypes are the A2 structure studied in this work and a B-type structure denoted B12, with a difference in formation energy of only 1.2 meV/atom favoring the latter [29]. Both are indirect-gap semiconductors, and while B12 provides a slightly better qualitative match to the experimental band structure [29], neither of them fits quantitatively the measured direct and indirect gaps [15, 16]. Further work is clearly needed to establish the stacking sequence in bulk BC<sub>2</sub>N samples, and the linear BPVE could be useful in this regard as it is only present in acentric (A-type) structures.

One intriguing possibility is that it may be possible to grow both polytypes of BC<sub>2</sub>N using current synthesis techniques. This has been achieved for other layered materials, such as transition metal dichalcogenides [41]. For example, bulk MoS<sub>2</sub> grows in two different polytypes, centrosymmetric 2H and noncentrosymmetric 3R, and the effects of inversion symmetry breaking can be clearly detected in the latter [42]. The reported energy difference

between them ranges from 0.1 to 2 meV/atom depending on the calculation [43–45], which is comparable to that between the B12 and A2 structures of BC<sub>2</sub>N [29]. We hope that our work will stimulate similar progress in graphitic BC<sub>2</sub>N, enabling the unambiguous identification of the A2 phase via its large and highly anisotropic photogalvanic effect.

*Acknowledgements* – We thank Stepan S. Tsirkin for sharing a computational code for the calculation of mirror band parities, and for a previous collaboration on related work. This work was supported by Grant No. FIS2016-77188-P from the Spanish Ministerio de Economía y Competitividad.

- 
- [1] V. I. Belinicher and B. I. Sturman, “The photogalvanic effect in media lacking a center of symmetry,” *Sov. Phys. Usp.* **23**, 199 (1980).
  - [2] B. I. Sturman and V. M. Fridkin, *The photovoltaic and photorefractive effects in noncentrosymmetric materials* (Gordon and Breach, 1992).
  - [3] V. M. Fridkin, “Bulk photovoltaic effect in noncentrosymmetric crystals,” *Crystallogr. Rep.* **46**, 654 (2001).
  - [4] W. Shockley and H. J. Queisser, “Detailed balance limit of efficiency of pn junction solar cells,” *J. Appl. Phys.* **32**, 510 (1961).
  - [5] J. Ma, Q. Gu, Y. Liu, J. Lai, P. Yu, X. Zhuo, Z. Liu, J.-H. Chen, J. Feng, and D. Sun, “Nonlinear photoresponse of type-II Weyl semimetals,” *Nat. Mater.* **18**, 476 (2019).
  - [6] L. Z. Tan, F. Zheng, S. M. Young, F. Wang, S. Liu, and A. M. Rappe, “Shift current bulk photovoltaic effect in polar materials – hybrid and oxide perovskites and beyond,” *npj Comput. Mater.* **2**, 16026 (2016).
  - [7] T. Rangel, B. M. Fregoso, B. S. Mendoza, T. Morimoto, J. E. Moore, and J. B. Neaton, “Large Bulk Photovoltaic Effect and Spontaneous Polarization of Single-Layer Monochalcogenides,” *Phys. Rev. Lett.* **119**, 067402 (2017).
  - [8] T. Morimoto and N. Nagaosa, “Topological nature of nonlinear optical effects in solids,” *Sci. Adv.* **2**, e1501524 (2016).
  - [9] B. M. Fregoso, T. Morimoto, and J. E. Moore, “Quantitative relationship between polarization differences and the zone-averaged shift photocurrent,” *Phys. Rev. B* **96**, 075421 (2017).
  - [10] F. de Juan, A. G. Grushin, T. Morimoto, and J. E. Moore, “Quantized circular photogalvanic effect in Weyl semimetals,” *Nat. Commun.* **8**, 15995 (2017).
  - [11] L. Z. Tan and A. M. Rappe, “Enhancement of the bulk photovoltaic effect in topological insulators,” *Phys. Rev. Lett.* **116**, 237402 (2016).
  - [12] Z. Yan, “Precise determination of critical points of topological phase transitions via shift current in two-dimensional inversion asymmetric insulators,” arXiv:1812.02191 [cond-mat] (2018), 1812.02191.
  - [13] G. B. Osterhoudt, L. K. Diebel, M. J. Gray, X. Yang, J. Stanco, X. Huang, B. Shen, N. Ni, P. J. W. Moll, Y. Ran, and K. S. Burch, “Colossal mid-infrared bulk photovoltaic effect in a type-I Weyl semimetal,” *Nat. Mater.* **18**, 471 (2019).

- [14] A. Y. Liu, R. M. Wentzcovitch, and M. L. Cohen, “Atomic arrangement and electronic structure of  $\text{BC}_2\text{N}$ ,” *Phys. Rev. B* **39**, 1760 (1989).
- [15] M. O. Watanabe, S. Itoh, T. Sasaki, and K. Mizushima, “Visible-light-emitting layered  $\text{BC}_2\text{N}$  semiconductor,” *Phys. Rev. Lett.* **77**, 187 (1996).
- [16] Y. Chen, J. C. Barnard, R. E. Palmer, M. O. Watanabe, and T. Sasaki, “Indirect band gap of light-emitting  $\text{BC}_2\text{N}$ ,” *Phys. Rev. Lett.* **83**, 2406 (1999).
- [17] M. O. Watanabe, T. Sasaki, S. Itoh, and K. Mizushima, “Structural and electrical characterization of  $\text{BC}_2\text{N}$  thin films,” *Thin Solid Films* **281**, 334 (1996).
- [18] M. O. Watanabe, S. Itoh, K. Mizushima, and T. Sasaki, “Electrical properties of  $\text{BC}_2\text{N}$  thin films prepared by chemical vapor deposition,” *J. Appl. Phys.* **78**, 2880 (1995).
- [19] M. O. Watanabe, S. Itoh, K. Mizushima, and T. Sasaki, “Bonding characterization of  $\text{BC}_2\text{N}$  thin films,” *Appl. Phys. Lett.* **68**, 2962 (1996).
- [20] H. Nozaki and S. Itoh, “Lattice dynamics of  $\text{BC}_2\text{N}$ ,” *Phys. Rev. B* **53**, 14161 (1996).
- [21] A. M. Cook, B. M. Fregoso, F. de Juan, S. Coh, and J. E. Moore, “Design principles for shift current photovoltaics,” *Nat. Commun.* **8**, 14176 (2017).
- [22] J. E. Sipe and A. I. Shkrebtii, “Second-order optical response in semiconductors,” *Phys. Rev. B* **61**, 5337 (2000).
- [23] N. Nagaosa, J. Sinova, S. Onoda, A. H. MacDonald, and N. P. Ong, “Anomalous Hall effect,” *Rev. Mod. Phys.* **82**, 1539 (2010).
- [24] R. von Baltz and W. Kraut, “Theory of the bulk photovoltaic effect in pure crystals,” *Phys. Rev. B* **23**, 5590 (1981).
- [25] V. I. Belinicher, E. L. Ivchenko, and B. I. Sturman, “Kinetic theory of the displacement photovoltaic effect in piezoelectrics,” *Sov. Phys. JETP* **56**, 359 (1982).
- [26] G. F. Bassani and G. P. Parravicini, “Band structure and optical properties of graphite and of the layer compounds  $\text{GaS}$  and  $\text{GaSe}$ ,” *Il Nuovo Cimento B* **50**, 95 (1967).
- [27] G. F. Bassani and G. P. Parravicini, *Electronic states and optical transitions in solids*, (Oxford, New York, Pergamon Press, 1975).
- [28] C. Wang, X. Liu, L. Kang, B.-L. Gu, Y. Xu, and W. Duan, “First-principles calculation of nonlinear optical responses by Wannier interpolation,” *Phys. Rev. B* **96**, 115147 (2017).
- [29] Z. Pan, H. Sun, and C. Chen, “Interlayer stacking and nature of the electronic band gap in graphitic  $\text{BC}_2\text{N}$ : First-principles pseudopotential calculations,” *Phys. Rev. B* **73**, 193304 (2006).
- [30] P. Giannozzi, S. Baroni, N. Bonini, M. Calandra, R. Car, C. Cavazzoni, D. Ceresoli, G. L. Chiarotti, M. Cococcioni, I. Dabo, A. Dal Corso, S. de Gironcoli, S. Fabris, G. Fratesi, R. Gebauer, U. Gerstmann, C. Gougoussis, A. Kokalj, M. Lazzeri, L. Martin-Samos, N. Marzari, F. Mauri, R. Mazzarello, S. Paolini, A. Pasquarello, L. Paulatto, C. Sbraccia, S. Scandolo, G. Sclauzero, A. P. Seitsonen, A. Smogunov, P. Umari, and R. M. Wentzcovitch, “QUANTUM ESPRESSO: a modular and open-source software project for quantum simulations of materials,” *J. Phys.: Condens. Matter* **21**, 395502 (2009).
- [31] J. P. Perdew, K. Burke, and M. Ernzerhof, “Generalized Gradient Approximation Made Simple,” *Phys. Rev. Lett.* **77**, 3865 (1996).
- [32] N. Marzari and D. Vanderbilt, “Maximally localized generalized Wannier functions for composite energy bands,” *Phys. Rev. B* **56**, 12847 (1997).
- [33] I. Souza, N. Marzari, and D. Vanderbilt, “Maximally localized Wannier functions for entangled energy bands,” *Phys. Rev. B* **65**, 035109 (2001).
- [34] A. A. Mostofi, J. R. Yates, Y.-S. Lee, I. Souza, D. Vanderbilt, and N. Marzari, “Wannier90: A tool for obtaining maximally-localised Wannier functions,” *Comput. Phys. Commun.* **178**, 685 (2008).
- [35] J. Ibañez-Azpiroz, S. S. Tsirkin, and I. Souza, “Ab initio calculation of the shift photocurrent by Wannier interpolation,” *Phys. Rev. B* **97**, 245143 (2018).
- [36] S. M. Young and A. M. Rappe, “First Principles Calculation of the Shift Current Photovoltaic Effect in Ferroelectrics,” *Phys. Rev. Lett.* **109**, 116601 (2012).
- [37] S. Y. Yang, J. Seidel, S. J. Byrnes, P. Shafer, C.-H. Yang, M. D. Rossell, P. Yu, Y.-H. Chu, J. F. Scott, J. W. Ager III, L. W. Martin, and R. Ramesh, “Above-bandgap voltages for ferroelectric photovoltaic devices,” *Nat. Nanotechnol.* **5**, 143 (2010).
- [38] Wei Ji, Kui Yao, and Yung C. Liang, “Evidence of bulk photovoltaic effect and large tensor coefficient in ferroelectric  $\text{BiFeO}_3$  thin films,” *Phys. Rev. B* **84**, 094115 (2011).
- [39] A. M. Glass, D. von der Linde, and T. J. Negran, “High-voltage bulk photovoltaic effect and the photorefractive process in  $\text{LiNbO}_3$ ,” *Appl. Phys. Lett.* **25**, 233 (1974).
- [40] X. Yang, K. Burch, and Y. Ran, “Divergent bulk photovoltaic effect in weyl semimetals,” arXiv:1712.09363 [cond-mat] (2017-12-26), 1712.09363.
- [41] J. A. Wilson and A. D. Yoffe, “The transition metal dichalcogenides discussion and interpretation of the observed optical, electrical and structural properties,” *Adv. Phys.* **18**, 193 (1969).
- [42] R. Suzuki, M. Sakano, Y. J. Zhang, R. Akashi, D. Morikawa, A. Harasawa, K. Yaji, K. Kuroda, K. Miyamoto, T. Okuda, K. Ishizaka, R. Arita, and Y. Iwasa, “Valley-dependent spin polarization in bulk  $\text{MoS}_2$  with broken inversion symmetry,” *Nat. Nanotechnol.* **9**, 611 (2014).
- [43] Y. Cheng, K. Yao, Y. Yang, L. Li, Y. Yao, Q. Wang, X. Zhang, Y. Han, and U. Schwingenschlögl, “Van der waals epitaxial growth of  $\text{MoS}_2$  on  $\text{SiO}_2/\text{Si}$  by chemical vapor deposition,” *RSC Advances* **3**, 17287 (2013).
- [44] J. Suh, T. L. Tan, W. Zhao, J. Park, D.-Y. Lin, T.-E. Park, J. Kim, C. Jin, N. Saigal, S. Ghosh, Z. M. Wong, Y. Chen, F. Wang, W. Walukiewicz, G. Eda, and J. Wu, “Reconfiguring crystal and electronic structures of  $\text{MoS}_2$  by substitutional doping,” *Nat. Commun.* **9**, 199 (2018).
- [45] X. B. Chen, Z. L. Chen, and J. Li, “Critical electronic structures controlling phase transitions induced by lithium ion intercalation in molybdenum disulphide,” *Chin. Sci. Bull.* **58**, 1632 (2013).